ARTICLE NO. 80-4129

Numerical Lifting Line Theory Applied to Drooped Leading-Edge Wings Below and Above Stall

John D. Anderson Jr.,* Stephen Corda,† and David M. Van Wie‡
University of Maryland, College Park, Md.

A numerical iterative solution to the classical Prandtl lifting-line theory, suitably modified for poststall behavior, is used to study the aerodynamic characteristics of straight rectangular finite wings with and without leading-edge droop. This study is prompted by the use of such leading-edge modifications to inhibit stall/spins in light general aviation aircraft. The results indicate that lifting-line solutions at high angle of attack can be obtained that agree with experimental data to within 20%, and much closer for many cases. Therefore, such solutions give reasonable preliminary engineering results for both drooped and undrooped wings in the poststall region. However, as predicted by von Kármán, the lifting-line solutions are not unique when sectional negative lift slopes are encountered. In addition, the present numerical results always yield symmetrical lift distributions along the span, in contrast to the asymmetrical solutions observed by Schairer in the late 1930's. Finally, a series of parametric tests at low angle of attack indicate that the effect of drooped leading edges on aircraft cruise performance is minimal.

I. Introduction

RECENT wind tunnel experiments[1-3] and flight tests, both radio controlled and full scale,[4,5] have demonstrated that certain leading-edge modifications can favorably tailor the high-lift characteristics of wings for light, single-engine general aviation airplanes so as to inhibit the onset of stall/spins. Since more than 30% of all general aviation accidents are caused by stall/spins, such modifications are clearly of practical importance. A modification of current interest is an abrupt extension and change in shape of the leading edge along a portion of the wing span—a so called "drooped" leading edge. This is shown schematically in Fig. 1, where at a given spanwise location, the chord and/or the leading-edge shape of the wing changes discontinuously. The net aerodynamic effect of this modification is a smoothing of the normally abrupt drop in lift coefficient C_L at stall, and the generation of a relatively large value of C_L at very high poststall angles of attack, as also shown in Fig. 1. As a result, an airplane with a properly designed drooped leading edge has increased resistance towards stall/spins.

In order to support and extend the results just mentioned, recent low-speed wind tunnel experiments at the University of Maryland[6-8] have shed new light on the basic aerodynamic flowfield over drooped and undrooped wings at high angles of attack. This includes the identification of a spanwise loop vortex and other complex three-dimensional flow interactions beyond the stall. Consequently, any detailed theoretical analysis or computation of the flowfield over wings at high angles of attack must clearly take into account such three-dimensional effects. No suitable analyses or computations exist today, and their future development will take some time.

On the other hand, it is advantageous to have a more immediate, although approximate, method for estimating the aerodynamic characteristics of drooped leading-edge wings. Such a method is provided by the classical Prandtl lifting-line theory, suitably modified for poststall behavior and solved by means of a numerical iterative technique to take into account nonlinear section lift vs angle-of-attack data. Therefore, the purpose of this paper is threefold: 1) to describe such a numerical lifting-line calculation; 2) to compare calculations with experimental data for drooped leading-edge wings for an angle-of-attack range from 0 to 50 deg; and 3) to give the results of a parametric study of the effects of leading-edge droop on low angle-of-attack cruise performance. This latter study is of interest because any practical leading-edge modification to inhibit stall/spins must not materially degrade the aerodynamic efficiency of the airplane during low angle-of-attack cruising flight.

Received Oct. 28, 1979; revision received Feb. 22, 1980.

Index categories: General Aviation; Aerodynamics, Computational Methods.

*Professor, Department of Aerospace Engineering. Associate Fellow AIAA.

†Student Assistant, Department of Aerospace Engineering; Glenn L. Martin Scholar.

‡Student Assistant, Department of Aerospace Engineering; R.M. Rivello Scholar.

II. Analysis

The classical Prandtl lifting line theory for low-speed incompressible flow has been in use since 1914, when it was developed by Ludwig Prandtl and Max Munk at Gottingen in Germany.[9] Its basic formulation can be found in any good aerodynamic text, e.g., Kuethe and Chow.[10] It postulates that a finite wing can be replaced by a bound spanwise vortex line (the lifting line) whose strength varies along the span, with a series of vortices that trail downstream. The strength of the bound vortex is given by $\Gamma(y)$ where Γ is the local circulation and y the coordinate along the span. The strength of each trailing vortex is $d\Gamma/dy$ evaluated at the given value of y at which the trailing vortex leaves the lifting line. The local bound vortex strength is related to the local lift per unit span L' through the Kutta-Joukowski law

$$L'(y) = \rho_\infty V_\infty \Gamma(y) \tag{1}$$

where ρ_∞ and V_∞ are freestream density and velocity, respectively. The effect of the trailing vortices is to induce a downwash velocity w at the lifting line, which in turn changes the angle of attack which the local airfoil section effectively sees. This change in angle of attack is the induced angle of attack α_i given by $\tan\alpha_i = w/V_\infty$. Hence, each local airfoil section along the span sees an effective angle of attack α_e that is related to α_i through

$$\alpha_e = \alpha - \alpha_i \tag{2}$$

where α is the usual geometric angle of attack. (See Ref. 11 for a basic discussion of finite wing definitions and

aerodynamic properties.) The induced angle of attack at any section y_s is related to the complete lift distribution (hence Γ distribution) over the span by

$$\alpha_i(y_s) = \frac{1}{4\pi V_\infty} \int_{-b/2}^{b/2} \frac{d\Gamma/dy}{(y_s - y)} dy \tag{3}$$

which is the basic equation of Prandtl's lifting-line theory.[9,10]

In the present paper, the preceding formulation is solved by means of a numerical iterative approach as follows:

1) For a given wing at a given α, first assume the lift distribution, i.e., assume a variation for $\Gamma(y)$. An elliptical lift distribution has been found satisfactory for this purpose.

2) With this assumed $\Gamma(y)$, evaluate Eq. (3) numerically at each of a preselected number of stations along the span. If the number of stations is $(k+1)$, then Simpson's rule applied to Eq. (3) gives

$$\alpha_i(y_s) = \frac{1}{4\pi V_\infty}\left(\frac{\Delta y}{3}\right) \sum_{n=2,4,6\ldots}^{k} \left\{ \frac{(d\Gamma/dy)_{n-1}}{(y_s - y_{n-1})} + 4\left[\frac{(d\Gamma/dy)_n}{y_s - y_n}\right] + \frac{(d\Gamma/dy)_{n+1}}{(y_s - y_{n+1})} \right\} \tag{4}$$

where Δy is the distance between stations. In Eq. (4), when $y_s = y_{n-1}$, y_n or y_{n+1} the singularity is avoided by replacing the given term by its average value based on the two adjacent sections. In any given calculation, the number of sections distributed along the span is at least 100, and for some cases as many as 200.

3) Using α_i from the preceding, obtain α_e at each station from Eq. (2).

4) With the distribution of α_e from step 3 obtain the sectional lift coefficient c_{l_s} from known airfoil data. Within the framework of lifting-line theory, each section of a finite wing is assumed to act as a two-dimensional airfoil at the local effective angle of attack α_e. The impact of this assumption on the present work will be discussed later.

5) From c_{l_s} obtained from step 4, a new circulation distribution is calculated from Eq. (1).

$$L'(y) = \rho_\infty V_\infty \Gamma(y) = \tfrac{1}{2}\rho_\infty V_\infty^2 c_s c_{l_s}$$

Hence,

$$\Gamma(y) = \tfrac{1}{2} V_\infty c_s c_{l_s} \tag{5}$$

where c_s is the local section chord.

6) This new distribution is compared with the values that were initially fed into step 2. If the results from step 5 do not agree with the input to step 2, then a new input is generated. If the previous input to step 2 is designated as Γ_{old}, and the result of step 5 is designated Γ_{new}, then the new input to step 2 is determined from

$$\Gamma_{input} = \Gamma_{old} + D(\Gamma_{new} - \Gamma_{old}) \tag{6}$$

Note that D is a damping factor for the iterations; a value of $D = 0.05$ was found to be optimum for the present calculations. Simply using Γ_{new} directly as the input to step 2 (i.e., setting $D = 1$) led to a divergent iteration; the iterative procedure required strong damping.

7) Steps 2-6 are repeated a sufficient number of cycles until Γ_{new} and Γ_{old} agree at each section to within 0.01% for a stretch of five previous iterations. This converged value of $\Gamma(y)$ then represents the solution for the lift distribution. For the present work, a minimum of 50 and sometimes as many as 150 iterations were required for convergence.

8) From the converged $\Gamma(y)$, the lift and induced drag coefficients, respectively, were obtained from

$$C_L = \frac{2}{V_\infty S} \int_{-b/2}^{b/2} \Gamma(y) dy \tag{7}$$

$$C_{D_i} = \frac{2}{V_\infty S} \int_{-b/2}^{b/2} \Gamma \sin\alpha_i dy \tag{8}$$

where S is the wing area. Equations (7) and (8) are evaluated by Simpson's rule.

The procedure just given generally works smoothly and quickly on a high-speed digital computer. Results from the present analysis are given in Fig. 2, which compares the present numerical lifting-line results with the theoretical values obtained by Prandtl[12] for rectangular wings with various aspect ratios. Agreement is excellent, hence verifying the integrity and accuracy of the present calculations.

The genesis of the preceding numerical technique reaches back to an obscure 1934 Japanese report by Tani,[13] who suggested a method of successive approximations to solve the lifting-line problem. Tani, and later Multhopp[14] used a series of multipliers to evaluate the downwash integral given by Eq. (3). This approach was systematized in 1947 by Sivells and Neely[15] to expedite slide rule or hand calculating machine use.

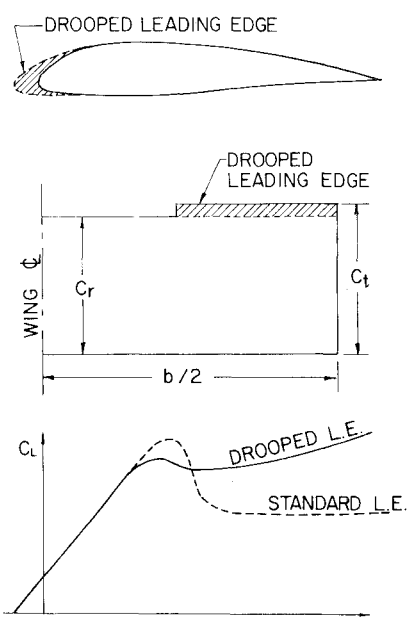

Fig. 1 Drooped leading-edge characteristics.

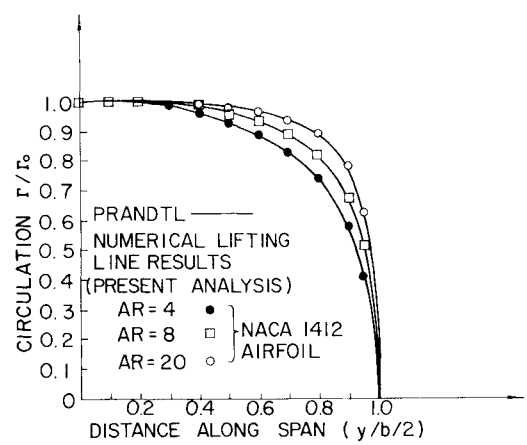

Fig. 2 Lift distributions for a rectangular wing; comparison between the theory of Prandtl and the present numerical lifting-line technique.

Only 10 stations per semispan were used. The next and most recent numerical solution was carried out by Weener[16] who studied the use of lifting-line theory for stalled or partially-stalled wings. Weener carried out a few digital solutions, but was unsatisfied by the results that were sometimes plagued by spanwise oscillations and divergent behavior. He subsequently carried out analog solutions for most of his cases. The present numerical lifting-line technique as described in steps 1-8 represents a logical and straightforward extension of the previous work, and demonstrates that digital computer solutions are indeed viable as long as a sufficient number of spanwise sections (say, 100 or more) are employed for accuracy and convergence. Moreover, such a numerical approach is absolutely necessary to study drooped leading-edge wings at high α, which involve highly nonlinear sectional lift data as well as geometric discontinuities along the span.

For the present calculations, the known sectional lift data used in step 4 was obtained from recent experimental measurements by Winkelmann and Barlow,[6] Saini,[7] and Agrawal[8] which included two-dimensional wings spanning the wind tunnel test section. These measurements provide the necessary airfoil data for angles of attack from 0 to 50 deg. It is only through such airfoil measurements that the present lifting-line technique can hope for any applicability beyond the stall. Indeed, Prandtl's basic lifting-line theory assumes that the flow is two-dimensional over each airfoil section and that the trailing vortices are in the plane of the freestream flow. These assumptions become less accurate as the angle of attack increases. However, Sears[17] has noted that the differences between Eq. (3) at stall and at low α are "quantitative differences, but the qualitative relationships must remain the same." The present authors feel that the greatest compromise in using lifting-line theory beyond the stall is that the "two-dimensional" airfoil data employed in step 4 is not truly two-dimensional. The measurements in Refs. 6-8 show strong three-dimensional flow characteristics beyond the stall even though the wing spans the entire test section. This is a characteristic of the viscous separated flow, and will influence any experimental data in the poststall region. At present, we see no way to circumvent this compromise; however, the results to be presented in Sec. III show that it is not fatal.

In the present analysis, the lifting line itself is conventionally assumed to be a continuous straight line perpendicular to the flow. For a planform as shown in Fig. 1 where the chord is extended over a portion of the span, strictly speaking the lifting line should have a discontinuous displacement forward in the extended region. The additional complications associated with such a broken lifting line are not considered worth the effort here, especially in light of the more serious assumptions just discussed above. Also, for practical applications, the leading edge is extended usually only about 10%, for which a straight lifting line ought to be a reasonable approximation.

Again, emphasis is made that the physical picture associated with classical lifting-line theory is a locally two-dimensional flow coupled with a single planar vortex sheet extending downstream from the wing trailing edge. This picture does not resemble the actual complex three-dimensional separated flow over wings at high angle of attack. Consequently, there is no theoretical reason to expect the poststall flow to be directly amenable to lifting-line analysis. However, if experimental airfoil section lift data beyond the stall is used in conjunction with a lifting-line calculation, there is hope in obtaining an "engineering solution" that gives reasonable poststall results. Such a philosophy is followed here, and the subsequent results verify the viability of the approach.

Finally, Sears[17] states that von Kármán noticed "some years ago" that Prandtl's lifting-line theory has nonunique solutions when the airfoil section has a negative lift slope, such as in the poststall region. Although unpublished, von Kármán is reported to have shown that infinitely many "eigendistributions" of $\Gamma(y)$, both symmetrical and asymmetrical, exist for any symmetrical planform. This was explored by Schairer[18] who found asymmetrical solutions only within a narrow range of α near the stall. Subsequently, Sears[19] found whole families of symmetrical and asymmetrical eigendistributions for the case of a negative lift slope. In the present work, nonunique solutions were also found beyond the stall; the final converged $\Gamma(y)$ in step 7 was found to depend on the initially assumed distribution in step 1. The practical impact of this nonunique nature is discussed in Sec. III. However, although many hundreds of different cases were run during the present investigation, many in the stall region and all for symmetrical planforms, no asymmetrical lift distributions were obtained. Without exception, all the converged distributions were precisely symmetrical for both drooped and undrooped wings. Even efforts to induce asymmetries by using an assumed asymmetrical initial distribution in step 1 resulted in a symmetrical converged solution in step 7. Since nothing in the present numerical technique forces symmetry, the present authors are led to wonder about the significance of such previously reported asymmetrical results. This presents an enigma worthy of future investigation.

III. Comparison with Experiment

A comparison between the present calculations and the measurements of Refs. 6-8 and 20 for a straight rectangular wing of aspect ratio $AR = 5.536$ and with an NACA 0015 airfoil section is given in Fig. 3. The circle and squares give the measured C_L for increasing and decreasing α, respectively. Note that in the stall region there is a hysteresis loop—even the experimental data is nonunique in the stall region. Such hysteresis effects have been commonly observed in airfoil and wing measurements for many years. Also in Fig. 3, the regular and inverted triangles give the numerical results for increasing and decreasing α, respectively. Here, the assumed initial lift distributions for the iterative solution at any given α are taken from the final converged solution at the previous α. The numerical curves were generated in 1 deg increments, starting at $\alpha = 0$, increasing to $\alpha = 47$ deg, and then decreasing back to $\alpha = 0$. Note that in the linear region at low α, and at very high α beyond 40 deg, unique solutions are obtained. However, between $\alpha = 10$ and 40 deg, where one or more sections of the finite wing see an effective angle of attack that falls on the negative lift slope of the input two-dimensional airfoil data, the numerical results are not unique. This produces a numerical hysteresis loop that has no direct physical connection with the experimental loop. However, the numerical data for increasing α agrees reasonably well with experiment in the prestall region, and that for decreasing α agrees somewhat with experiment in the poststall region. However, in general, the comparison shown in Fig. 3 is not as good as desired.

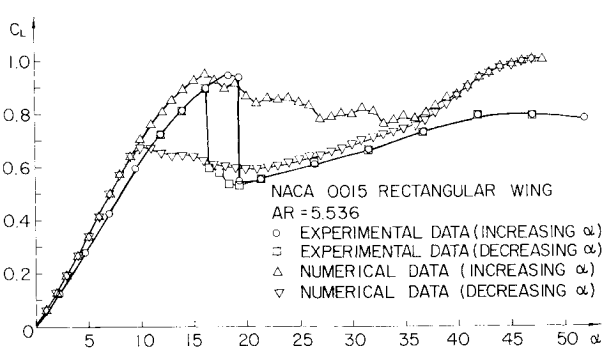

Fig. 3 Lift coefficient vs angle of attack for a rectangular wing with an NACA 0015 airfoil; comparison between experiment[7] and the present numerical technique.

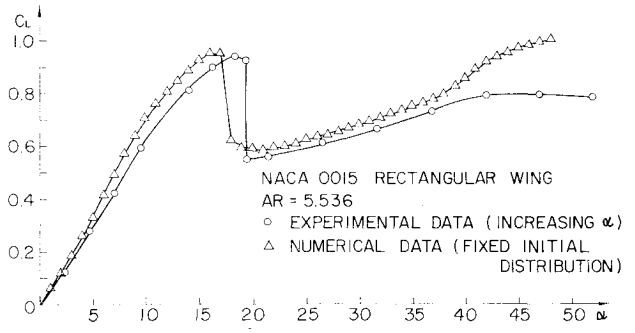

Fig. 4 Lift coefficient vs angle of attack; comparison between experiment[7] and numerical results.

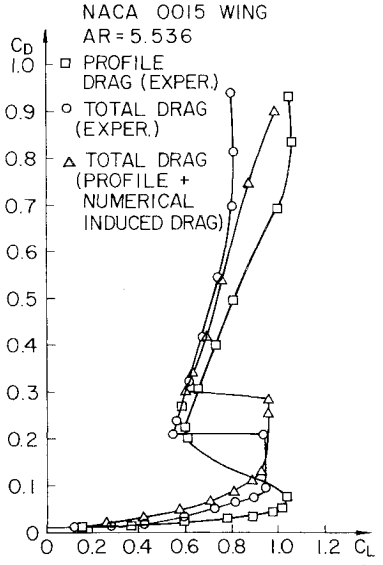

Fig. 5 Drag polar; comparison between experiment[7] and numerical results.

A different approach is taken in Fig. 4. Here, the same experimental data is shown, but the numerical results are obtained by assuming the same initial lift distribution at the beginning of the iterations for each angle of attack. That is, each triangle in Fig. 4 is a converged result that started with the same initial distribution. This fixed initial distribution was assumed to be elliptical, with a value of $\Gamma/V_\infty c = 0.438$ at midspan. Note that reasonable agreement (within about 10%) is obtained between theory and experiment except above α = 40 deg. Therefore, all subsequent comparisons are made with the numerical results using the same fixed initial lift distribution as just described.

The corresponding drag polar results for $\alpha = 0$-50 deg are given in Fig. 5. Here, experimental measurements of profile drag (for the two-dimensional wing) and total drag for the finite wing are shown. Note the S-shaped drag polars that are caused by the high angle-of-attack variations. The numerical data for total drag is obtained by adding the experimental profile drag and calculated induced drag at each section, and integrating over the entire wingspan. Again, reasonable agreement between theory and experiment is obtained.

Results for drooped leading-edge wings are compared in Figs. 6 and 7 for $c_t/c_r = 1.08$ and 1.2, respectively. The root section for both wings was an NACA 0015 airfoil, whereas the tip sections in Figs. 6 and 7 are NACA 0014.6 and 0014.2 airfoils, respectively. These rather odd airfoil sections resulted simply from the necessary chord extensions and the desire to have both the root and tip airfoil shapes to fare smoothly into each other at the spanwise location of the droop discontinuity. The droop occurs at mid-semispan. Note that

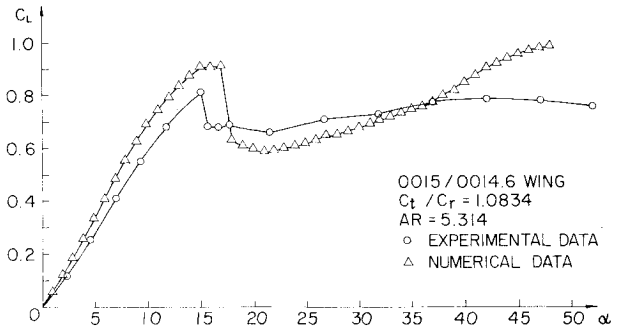

Fig. 6 Lift coefficient vs angle of attack for a drooped leading-edge wing; comparison between experiment[7] and numerical results.

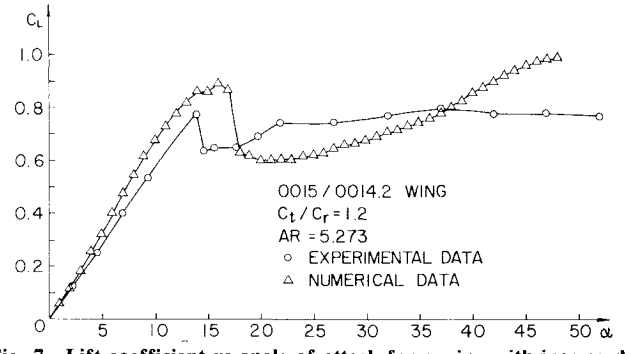

Fig. 7 Lift coefficient vs angle of attack for a wing with increased leading-edge droop; comparison between experiment[7] and numerical results.

the comparisons between numerical and experimental results are somewhat tenuous but the differences are no more than 20% over much of the angle-of-attack range.

In general, surveying Figs. 4-7, we note that the numerical results do not predict stall at the correct α and yield a higher lift slope in the linear region than experiment. However, the experimental data were obtained from finite wings mounted on one wall of the wind tunnel,[6-8,20] so-called "reflection plane" models. Hence, the tunnel wall boundary layer flowing over the wing root section effectively reduces the aspect ratio seen by the mainstream. In turn, this will cause the experimental data to see a smaller lift slope. The measured data in Figs. 4-7 are not corrected for this effect and, therefore, the comparisons in the low α linear lift region are at least qualitatively explained.

It is of interest to inspect the numerical lift distributions obtained for the drooped leading-edge wings. For the wing with $c_t/c_r = 1.08$, the distributions of $\Gamma(y)$ for $\alpha = 8$ and 16 deg are given in Fig. 8. Note that at high α the distribution shows a major dip and oscillation in the vicinity of the droop discontinuity, whereas at lower α it is virtually unaffected. The experimental data of Refs. 6-8 and 20 have clearly identified a downstream flowing vortex generated at the discontinuity. The dip shown in Fig. 8 is a numerical indication of this vortex. However, the oscillations in the vicinity of the dip may be numerical, although they do not correspond to adjacent sections (for these results, $\Delta y = 0.023$ ft).

In general, the results of this section indicate that the viability of the current numerical lifting-line solutions for prediction of drooped and undrooped finite wing lift and drag at high angles of attack is a matter of interpretation and philosophy. If one is interested in close agreement between experiment and theory, then lifting-line results are not good. On the other hand, if one is interested in a relatively quick and easy engineering estimate of the properties of such wings, then the lifting-line technique as presented here appears to give results within 20%, and many times much closer.

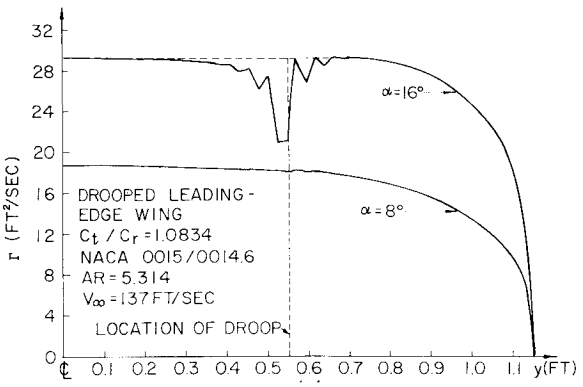

Fig. 8 Numerical lift distributions for a drooped leading-edge wing.

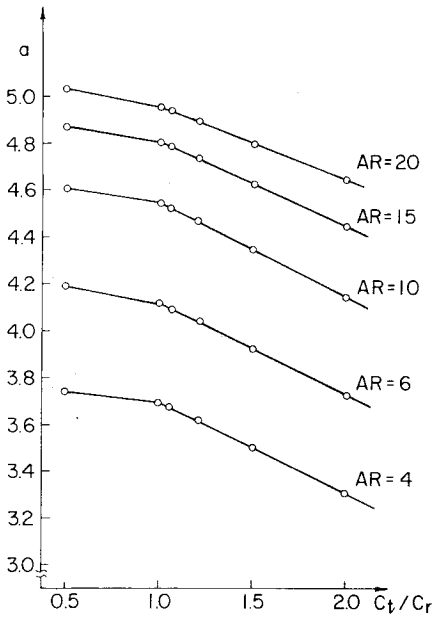

Fig. 9 Effect of chord discontinuity on lift slope; numerical results.

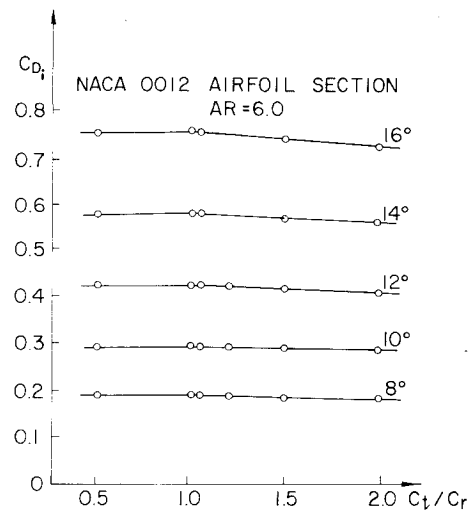

Fig. 10 Effect of chord discontinuity on drag coefficient; numerical results.

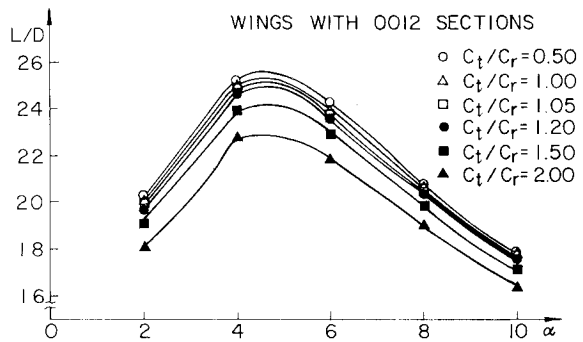

Fig. 11 Effect of chord discontinuity on lift/drag ratio for wings with an NACA 0012 section; numerical results.

IV. Parametric Studies at Low Angle of Attack

The purpose of this section is to address the question: How much does leading-edge droop affect low angle-of-attack cruise performance? From the results of Sec. III, the current lifting-line technique should be a valid tool to study this question especially since we are dealing with the essentially linear prestall region. Therefore, in this section lifting-line results are presented for three parametric variations: relative tip-to-root chord ratio; the spanwise location of the droop; and major discontinuities in airfoil shape. All the wing planforms considered here are of the basic, straight, rectangular geometry shown in Fig. 1; swept and/or tapered wings are not considered.

Effect of Tip-to-Root Chord Ratio

The influence of a discontinuous change of chord length at mid-semispan ($b/4$) on lift slope is shown in Fig. 9. Note that the lift slope, $a \equiv dC_L/d\alpha$, monotonically decreases as c_t/c_r increases, for the same aspect ratio, $\mathcal{R}$. The aspect ratio for the drooped leading-edge wings is still conventionally defined as $\mathcal{R} = b^2/S$. The corresponding induced drag coefficient is given in Fig. 10; note that C_{D_i} is virtually unaffected by c_t/c_r. The consequent effects on L/D are illustrated in Fig. 11 for $\mathcal{R} = 6$. These results indicate that, in comparison to a straight undrooped wing ($c_t/c_r = 1.0$), a wing with $c_t/c_r = 1.05$ (characteristic of current flight tests[4,5]) will suffer only a 0.6% decrease in maximum L/D, and for $c_t/c_r = 1.2$, the decrease in $(L/D)_{max}$ will be 1.2%. Also, note that higher L/D ratios are obtained when the root chord is larger than the tip chord, $c_t/c_r < 1.0$. This trend is in conflict with the effects of droop on the stall/spin behavior,[4] which is improved by extending the tip chord, $c_t/c_r > 1.0$.

It is interesting to examine the effect of c_t/c_r on lift distribution. This is illustrated in Fig. 12. Obviously as c_t/c_r is increased, the outer portion of the wing is increasingly loaded. Also, note the oscillations in the region of the planform discontinuity.

Effect of Spanwise Location

Lift/drag ratios for three different spanwise locations of the droop are given in Fig. 13. Note that $(L/D)_{max}$ is increased by moving the droop location closer to the wing tips. However, a shift from ¼ semispan to ¾ semispan changed the $(L/D)_{max}$ by only 1.2%.

Effect of Airfoil Shape Discontinuity

Figure 14 contains L/D results for a wing composed of NACA 0012 and 4412 airfoils joined at different spanwise locations; there is no discontinuity in planform ($c_t/c_r = 1.0$). The circles give results for a completely 0012 wing, and the inverted triangles are for a completely 4412 wing. For the intermediate composite shapes, the L/D curves are predictable averages of the two different airfoils. There are no surprises here. However, note that a major change in airfoil shape causes a major change in L/D ratio that far exceeds the influence of the previous parameters already described.

In summary, for the leading-edge droop configurations currently in flight,[4,5] the present results show only a minimal

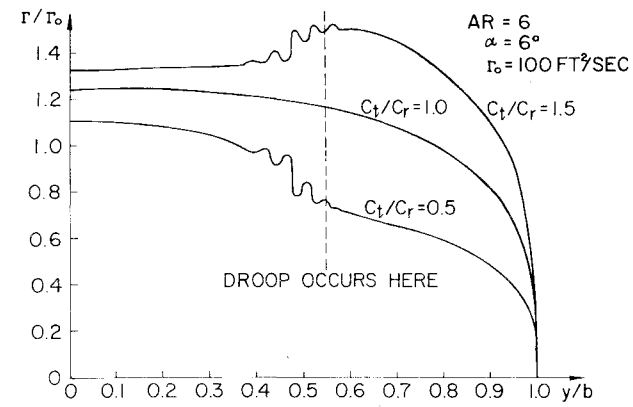

Fig. 12 Effect of chord discontinuity on lift distribution; numerical results.

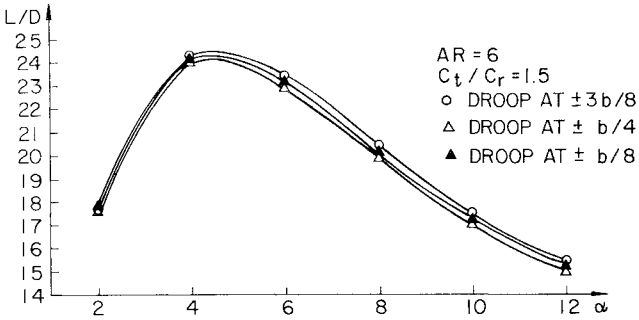

Fig. 13 Effect of different spanwise locations of droop; numerical results.

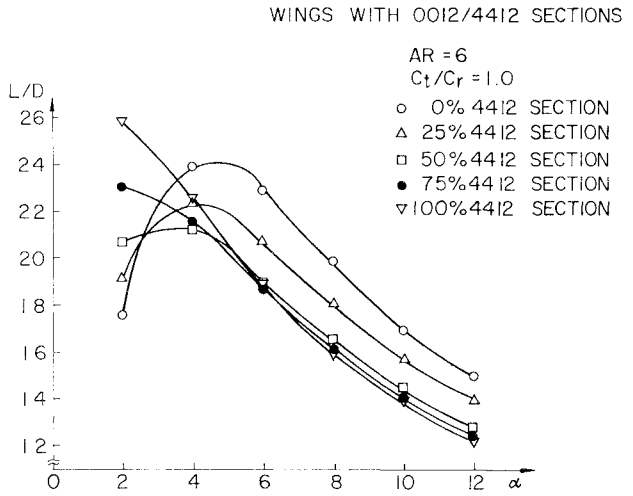

Fig. 14 Effect of a discontinuity in airfoil shape; numerical results.

effect on aircraft cruise performance. There appears to be no deleterious effect as long as $c_t/c_r < 1.2$. Indeed, for $c_t/c_r < 1.0$, there is a marginal improvement of L/D compared to the standard wing. However, the reader is cautioned that lifting-line theory does not take into account the local viscous flow effects of a drooped leading-edge discontinuity on local flowfield separation and transition at low angle of attack. On the other hand, these effects may only be local, and will most likely not materially affect the conclusion just mentioned.

V. Conclusions

A numerical solution of Prandtl's classical lifting-line theory, suitably modified for poststall behavior, is used to study the characteristics of drooped leading-edge wings. The major conclusions of this study are:

1) Lifting-line solutions at high angle of attack can be obtained that agree with experimental data to within 20%, and much closer for many cases. Therefore, such solutions appear to give reasonable preliminary engineering results for the high angle-of-attack poststall region for both drooped and undrooped wings.

2) The solutions exhibit nonuniqueness when sectional negative lift slopes are encountered. This is consistent with earlier predictions by von Kármán.

3) However, in contradistinction to previous predictions, asymmetrical lift distributions for symmetrical planforms in the stall region were not observed. Without exception, for the many hundreds of cases run in the present study, the resulting lift distributions were always precisely symmetrical.

4) Low angle-of-attack parametric studies show that the effects of tip-to-chord ratio and spanwise location of the leading-edge droop have minimal effect on $(L/D)_{max}$, and hence the aircraft's cruise performance. However, the effect of a discontinuous change in airfoil shape yielded a major change in L/D. The resulting composite wing characteristics are a predictable average of the two airfoil characteristics.

5) Finally, it is wise not to stretch the applicability of lifting-line theory too far. For the high angle-of-attack cases presented here, the flow is highly three dimensional, and only an appropriate three-dimensional flowfield calculation can hope to predict the detailed aerodynamic properties of such flows.

Acknowledgments

This work was supported by both NASA Grant NS G1570 with Daniel J. DiCarlo as technical monitor, and by the Minta Martin Fund for Aeronautical Research, an endowment fund given to the College of Engineering, University of Maryland, by the late Glenn L. Martin.

References

[1] Kroeger, R.A. and Feistel, T.W., "Reduction of Stall-Spin Entry Tendencies Through Wing Aerodynamic Design," SAE Paper 760481, presented at the Business Aircraft Meeting, Wichita, Kan., April 1976.

[2] Feistel, T.W., Anderson, S.B., and Kroeger, R.A., "A Method for Localizing Wing Flow Separation at Stall to Alleviate Spin Entry Tendencies," AIAA Paper 78-1476, presented at the AIAA Aircraft Systems and Technology Conference, Los Angeles, Calif., Aug. 1978.

[3] Anderson, S.B., "Historical Overview of Stall/Spin Characteristics of General Aviation Aircraft," *Journal of Aircraft*, Vol. 16, July 1979, pp. 455-461.

[4] DiCarlo, D.J. and Johnson, J.L., Jr., "Exploratory Study of the Influence of Wing Leading-Edge Modifications on the Spin Characteristics of a Low-Wing Single-Engine General Aviation Airplane," AIAA Paper 79-1837, presented at the AIAA Aircraft Systems and Technology Meeting, N.Y., Aug. 1979.

[5] Stough, H.P., III and Patton, J.M., Jr., "The Effect of Configuration Changes on Spin and Recovery Characteristics of a Low-Wing Spin Research Airplane," AIAA Paper 79-1786, presented at the AIAA Aircraft Systems and Technology Meeting, N.Y., Aug. 1979.

[6] Winkelmann, A.W. and Barlow, J.B., "A Flowfield Model for a Rectangular Planform Wing Beyond Stall," *AIAA Journal*, Vol. 18, Aug. 1980, pp. 1006-1008.

[7] Saini, J.K., "An Experimental Investigation of the Effects of Leading Edge Modifications on the Post-Stall Characteristics of an NACA 0015 Wing," M.S. Thesis, Dept. of Aerospace Engineering, Univ. of Maryland, July 1979.

[8] Agrawal, S., "Parametric Studies of Discontinuous Leading-Edge Effects on Wing Characteristics for Angles-of-Attack up to 50°," M.S. Thesis, Dept. of Aerospace Engineering, Univ. of Maryland, July 1979.

[9] Durand, W.F., ed., *Aerodynamic Theory*, Vols. I and II, Julius Springer, Berlin, 1935.

[10] Kuethe, A.M. and Chow, C.Y., *Foundations of Aerodynamics,* 3rd Ed., John Wiley, 1976.

[11] Anderson, J.D., Jr., *Introduction to Flight,* McGraw-Hill, 1978.

[12] Prandtl, L. and Tietjins, O.G., *Applied Hydro- and Aeromechanics,* United Engineering Trustees, Inc., 1934. (Also, Dover Publications, Inc., 1957.)

[13] Tani, I., "A Simple Method of Calculating the Induced Velocity of a Monoplane Wing," Rept. 111, Aeronautical Research Institute, Tokyo Imperial Univ., Aug. 1934.

[14] Multhopp, H., "Die Berechnung der Auftriebsverteilung von Tragflugein," Luftfahrtforschung Bd. 15, Nr. 14, April 1938, pp. 153-169.

[15] Sivells, J.C. and Neely, R.H., "Method for Calculating Wing Characteristics by Lifting-Line Theory Using Nonlinear Section Lift Data," NACA TN 1269, April 1947.

[16] Weener, E.F., "Stalled and Partially Stalled High Aspect Ratio Straight Wings," Ph.D. Dissertation, Dept. of Aerospace Engineering, Univ. of Michigan, 1975.

[17] Sears, W.R., "Some Recent Developments in Airfoil Theory," *Journal of Aeronautical Sciences,* Vol. 23, May 1956, pp. 490-499.

[18] Schairer, R.S., "Unsymmetrical Lift Distributions on a Stalled Monoplane Wing," M.S. Thesis, California Institute of Technology, 1939.

[19] Sears, W.R., "A New Treatment of the Lifting-Line Wing Theory, With Applications to Rigid and Elastic Wings," *Quarterly of Applied Mathematics,* Vol. 6, Oct. 1948, pp. 239-255.

[20] Winkelmann, A.E., Barlow, J.B., Agrawal, S., Saini, J.K., Anderson, J.D., Jr., and Jones, E., "The Effects of Leading Edge Modifications on the Post-Stall Characteristics of Wings," AIAA Paper 80-0199, presented at the AIAA 18th Aerospace Sciences Meeting, Jan. 1980.